ELSEVIER

Contents lists available at ScienceDirect

Materials Science & Engineering A

journal homepage: http://www.elsevier.com/locate/msea





Microstructure, mechanical properties and creep behaviour of extruded Zn-xLi ($x=0.1,\,0.3$ and 0.4) alloys for biodegradable vascular stent applications

Suming Zhu^a, Chengcheng Wu^a, Guannan Li^b, Yufeng Zheng^{b,**}, Jian-Feng Nie^{a,*}

- ^a Department of Materials Science and Engineering, Monash University, Victoria, 3800, Australia
- b Department of Materials Science and Engineering, College of Engineering, Peking University, Beijing, 100871, China

ARTICLE INFO

Keywords: Zn-Li alloys Microstructure Mechanical properties Creep mechanisms Grain boundary sliding

ABSTRACT

Zn–Li alloys have been shown to be promising for biodegradable vascular stent applications due to their favourable biocompatibility and superior strength. This work presents a thorough evaluation of the microstructure, room temperature mechanical properties and human body temperature creep behaviour of hotextruded Zn-xLi ($x=0.1,\,0.3$ and 0.4) alloys. All alloys show typical basal texture after the extrusion but the recrystallized grains are much finer with increasing Li content. Consequently, not only the room temperature yield and tensile strengths but also the elongation to fracture is significantly increased with increasing Li content. However, increasing Li content has an adverse effect on the creep resistance at human body temperature. Moreover, there is a transition in the operative creep mechanism from dislocation creep in the Zn-0.1Li alloy to grain boundary sliding in the Zn-0.3Li and Zn-0.4Li alloys. The observed mechanical behaviour in these alloys can be well related to the grain size effect, i.e. strengthening to softening by grain boundaries with decreasing strain rate. This work suggests that grain size of biodegradable zinc alloys should be optimized in order to achieve a balance between room temperature mechanical properties and human body temperature creep resistance.

1. Introduction

As biodegradable metallic materials, magnesium (Mg) and iron (Fe) based alloys have received tremendous research on tailoring mechanical properties and corrosion performance to meet the requirements for vascular stent applications [1,2]. In recent years, zinc (Zn) based alloys have emerged as another family of biodegradable material due to promising biocompatibility and biodegradability [3,4]. Like Mg and Fe, Zn is also an essential element in human nutrition but has an intermediate corrosion potential between Fe and Mg [5]. The binary Zn alloys studied so far include Zn-Li [6–8], Zn-Mg [9–13], Zn-Ca [12], Zn-Mn [14,15], Zn-Cu [16,17], Zn-Ag [18] and Zn-Zr [19].

Li was proposed as a promising alloying element to Zn by Zhao et al. [6,7]. Zhao et al. [6] investigated the mechanical properties and the in vivo biodegradability and biocompatibility of Zn-0.1Li (wt. %) alloy wires fabricated by hot extrusion and drawing. It was found that alloying of 0.1% Li increased the yield strength from 86 ± 14 MPa (pure Zn) to

 238 ± 60 MPa with an elongation of $17 \pm 7\%$. The Zn-0.1Li alloy had a moderate low degradation rate and a moderate inflammation with a non-obstructive neointima, which are similar to the in vivo biodegradability and biocompatibility of pure Zn. Zhao et al. [7] also studied the structural characteristics, mechanical properties and in vitro corrosion performance of hot-rolled Zn-0.2Li, Zn-0.4Li and Zn-0.7Li alloys, which correspond to the hypoeutectic, eutectic and hypereutectic compositions, respectively. It was shown that the alloying of Li led to the formation of LiZn₄ intermetallic phase and an improvement in strength, but there was a severe decrease in ductility when the addition of Li was above the eutectic composition. It was thus suggested that Li additions into Zn should not exceed 0.4%. Similar in vivo corrosion performance to pure Zn was found for the hot-rolled Zn-0.2Li and Zn-0.4Li alloys. Dai et al. [8] evaluated the microstructure and mechanical properties of hot-extruded pure Zn and Zn-0.5Li alloy. It was shown that both strength and ductility were improved by the addition of 0.5% Li to pure Zn, with the tensile strength increased from 125.6 MPa to 364.9 MPa and the

E-mail addresses: yfzheng@pku.edu.cn (Y. Zheng), jianfeng.nie@monash.edu (J.-F. Nie).

^{*} Corresponding author.

^{**} Corresponding author.

elongation increased from 15% to 22%. The strength improvement in the Zn-0.5Li alloy was attributed to the grain refinement and precipitation of nano-sized $LiZn_4$ precipitates.

This work presents a systematic study of the microstructure, room temperature mechanical properties and human body temperature creep performance of a series of extruded Zn-xLi (x = 0.1, 0.3 and 0.4) alloys. Creep performance is evaluated here because it has long been known that pure Zn and Zn alloys can undergo creep deformation at room temperature [20–22], which is actually a high homologous temperature (\sim 0.43 of the melting temperature). The creep and rupture properties of the extruded Zn-0.1Li alloy have been briefly reported by the current authors [23]. The present paper focuses on the effect of increasing Li content on microstructure and its relationship with mechanical behaviour. The understanding gained from this work should be helpful for the design and processing of Zn alloys for biodegradable vascular stent applications.

2. Experimental details

Alloys with nominal compositions of Zn-0.1Li, Zn-0.3Li and Zn-0.4Li (wt.%) were cast into ingots from high purity pure Zn and Zn-5Li master alloy by induction melting under the protection of mixed gas of SF₆ (1 vol%) and CO₂ (balance). Cylindrical blocks of 40 mm in diameter were cut from the ingots and were extruded at 300 $^{\circ}\text{C}$ into billets of 10 mm in diameter, corresponding to an extrusion ratio of about 16:1. Cylindrical specimens with a gauge length of 16 mm and a diameter of 3.5 mm were machined from the extruded billets for mechanical testing. Room temperature mechanical properties were evaluated by tensile testing using a screw-driven Instron machine. The crosshead speed employed was 1 mm/min, corresponding to a nominal strain rate of 1×10^{-3} s⁻¹. Creep resistance was evaluated by constant-load tensile creep tests at 37 °C, a typical human body temperature. The creep specimens were heated by immersing into heated oil baths, with the temperature controlled to within ± 1 °C. The creep strain was measured by an extensometer that was attached directly to the gauge section of the specimens. While most creep tests were run until the specimens ruptured or were stretched to the limit of the creep rig, some tests were interrupted after running for 500 h.

Microstructural features in the extruded alloys were characterized by scanning electron microscopy (SEM) and electron backscatter diffraction (EBSD) using a JEOL 7001 FEG SEM machine equipped with an Aztec analysis system. The EBSD samples were prepared by electropolishing either in a solution containing 5.3 g lithium chloride, 11.16 g magnesium perchlorate, 500 ml methanol and 100 ml 2-butoxy-ethanol at $-45\ ^{\circ}\text{C}$ and a voltage of 100 V or in a solution containing 33 vol%

orthophosphoric acid and 67 vol% ethanol at room temperature and a voltage of 3 V. From the EBSD orientation maps, grain size of the extruded alloys was determined by the mean linear intercept method (ASTM Standard E112) implemented in Oxford Instruments HKL Channel 5 software. SEM was also employed to examine the specimen fracture surfaces after the room temperature tensile tests and human body temperature creep tests.

3. Results

3.1. As-extruded microstructure

The SEM microstructural observations of the Zn–Li alloys along the extrusion direction are shown in Fig. 1. All alloys are characterized by equiaxed grains and stringers of intermetallic phase (presumably LiZn₄ according to the binary Li–Zn phase diagram [24]) aligned along the extrusion direction, which are typical of fully recrystallized extrusion microstructure. With increasing Li content, it appears that the LiZn₄ phase fraction is increased while the grain size is significantly reduced, indicating that the LiZn₄ phase facilitates the dynamic recrystallization of Zn, most likely by the particle stimulated nucleation (PSN) [25]. The operation of PSN is clearly evidenced by a bi-modal grain structure in the 0.1Li alloy, with fine grains being associated with the stringers of the LiZn₄ phase. The bi-modal grain structure is less apparent in the 0.3Li and 0.4Li alloys as a result of increased PSN.

The EBSD orientation maps and inverse pole figures of the Zn–Li alloys perpendicular to the extrusion direction are shown in Fig. 2. The bi-modal grain structure in the 0.1Li alloy is verified by the orientation map (Fig. 2a). The grain size determined from the orientation maps is $21.7\pm11.3,\,6.4\pm1.7$ and $5.9\pm1.4\,\mu m$ for the 0.1Li and 0.3Li and 0.4Li alloys, respectively. It is noted that all alloys have developed the typical (0001) fibre texture, i.e. the c-axis of grains is aligned perpendicular to the extrusion direction. The (0001) fibre texture is slightly weaker in the 0.3Li and 0.4Li alloys as compared with the 0.1Li alloy. This seems to provide further support for the operation of PSN in these alloys since PSN tends to waken the recrystallization texture [25].

3.2. Room temperature mechanical properties

Room temperature tensile curves of the Zn–Li alloys are shown in Fig. 3 and the yield strength, tensile strength and elongation to failure determined from the tensile curves are listed in Table 1. It is noted that the elastic region is not linear in these alloys, in particular for the 0.3Li and 0.4Li alloys. Such nonlinear elasticity has been observed in other hcp metals or alloys, such as uranium [26], zirconium [27] and cast

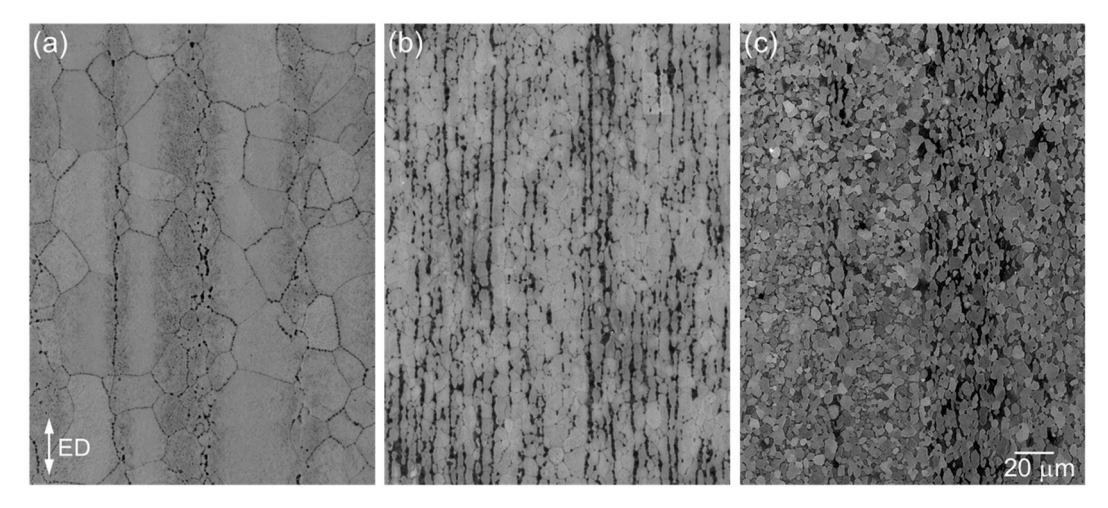


Fig. 1. SEM secondary electron images showing the grain structure and stringers of intermetallic phase (dark contrast) along the extrusion direction (ED) in the (a) Zn-0.1Li [23], (b) Zn-0.3Li and (c) Zn-0.4Li alloys. Note the increase in intermetallic phase fraction while the decrease in matrix grain size with increasing Li content.

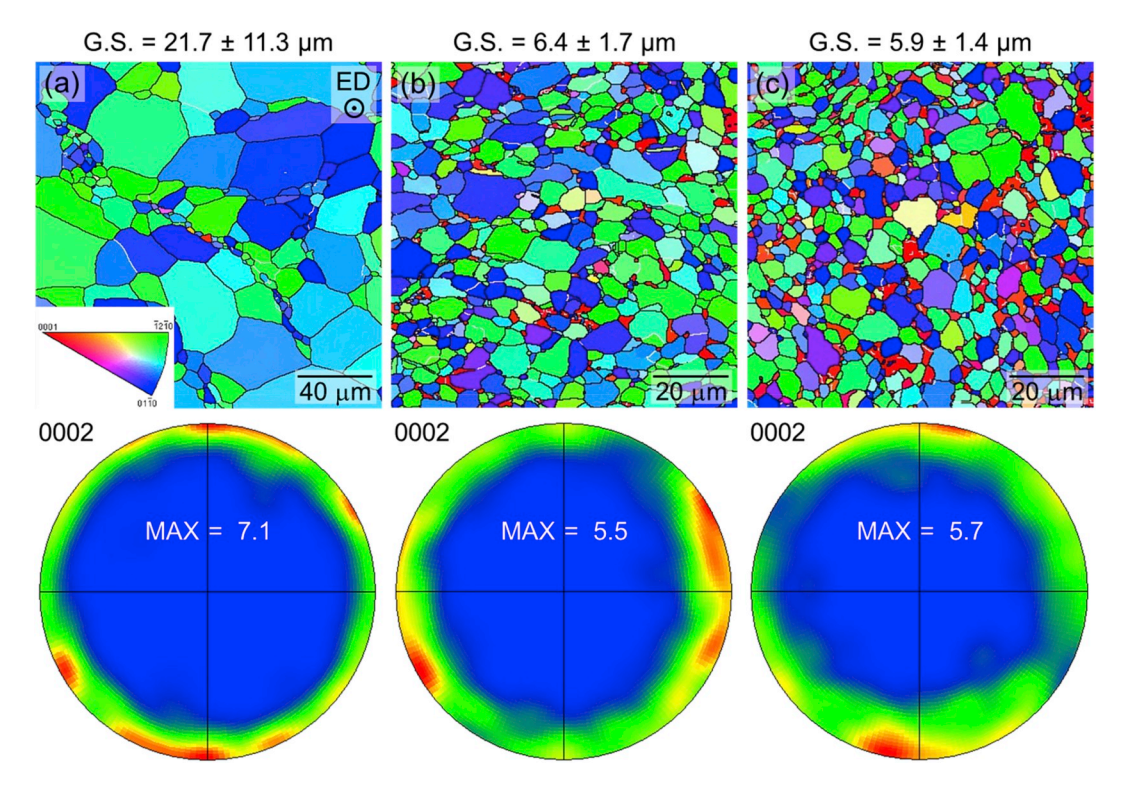


Fig. 2. EBSD orientation maps and inverse pole figures perpendicular to ED for the (a) Zn-0.1Li [23], (b) Zn-0.3Li and (c) Zn-0.4Li alloys. The red features in the orientation maps should be LiZn₄ phase, but somehow were incorrectly identified by the Aztec analysis software as Zn grains with [0001] orientation. These [0001] grains were excluded from the inverse pole figures and grain size measurements. (For interpretation of the references to colour in this figure legend, the reader is referred to the Web version of this article.)

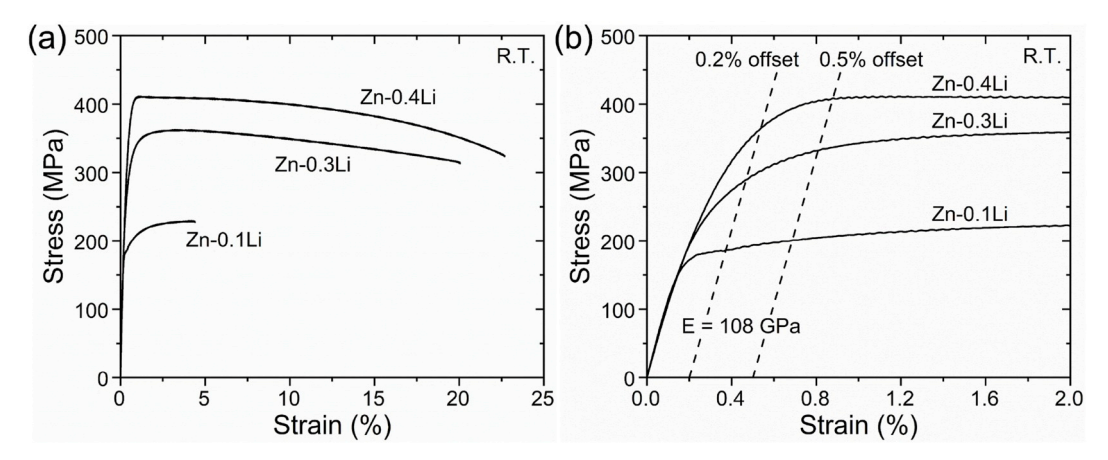


Fig. 3. Room temperature tensile curves of the Zn–Li alloys in the (a) whole range and (b) initial stage. The 0.2% and 0.5% offset strains are indicated by dashed lines with gradient 108 GPa in (b). Note the anelastic behaviour in these alloys, which is more pronounced in the 0.3Li and 0.4Li alloys.

 Table 1

 Room temperature tensile properties of the Zn-Li alloys.

Zn-0.1Li 189.1 \pm 4.7 202.9 \pm 3.0 230.2 \pm 0.4 [23]	
	4.0 ± 0.6
Zn-0.3Li 292.0 \pm 3.9 335.2 \pm 4.3 367.2 \pm 6.5 Zn-0.4Li 363.7 \pm 9.1 398.5 \pm 9.1 405.3 \pm 7.0	$19.3 \pm 0.9 \\ 27.4 \pm 10.8$

magnesium alloys [28–30], and is termed as anelasticity or pseudoelasticity. The anelasticity is generally caused by twinning, which is partially reversible upon unloading. With the presence of anelasticity, the yield strength determined using the conventional 0.2% offset method is underestimated. To account for the anaelsticity, using a higher offset (e.g. 0.5%) can give a more approximate estimation of yield strength than using the conventional 0.2% offset [29]. In this study, for the purpose of comparison, both 0.2% yield strength and 0.5% yield strength are measured for the three alloys (Fig. 3b and Table 1). Apparently, the 0.1Li alloy has the lowest strength properties and also the lowest ductility, with an elongation of only $\sim\!4.0\%$. It is interesting to see that increasing Li content not only increases the strength properties but also leads to an improvement in ductility. Consequently, both 0.3Li and 0.4Li alloys readily meet the benchmark mechanical properties required for vascular stent materials, i.e. yield strength >200 MPa, ultimate tensile strength >300 MPa, elongation >15–18% [31]. However, it should be noted that, while the 0.1Li alloy exhibits pronounced

strain hardening, the strain hardening appears to be modest in the 0.3Li and 0.4Li alloys.

The SEM fractographs of the Zn–Li alloys after room tensile testing are shown in Fig. 4. Apparently, the 0.1Li alloy is dominated by transgranular cleavage fracture, a typical brittle fracture mode for pure Zn with large grains [32–34]. The cleavage fracture is consistent with the low ductility of the 0.1Li alloy. For the 0.3Li and 0.4Li alloys, the fracture appears to be a mixture of transgranular cleavage fracture and ductile dimple fracture. The mixed cleavage and dimple fracture has been observed in fine-grained Zn–Al, Zn–Mg and Zn–Mn alloys [11,14].

3.3. Creep behaviour at human body temperature

Typical creep curves for the 0.3Li and 0.4Li alloys are shown in Fig. 5, where three stages are identified, i.e. the primary stage in which the creep rate decreases with increasing creep time, the secondary stage in which the creep rate remains steady and the tertiary stage in which the creep rate increases with time until fracture. Similar to the 0.1Li alloy, the 0.3Li and 0.4Li alloys exhibit very limited secondary creep stage, followed by an "extended period of tertiary creep" [35]. However, it is worth noting that the primary stage is also very limited in the 0.3Li and 0.4Li alloys, which is in contrast to the 0.1Li alloy in which a fair amount of primary creep is observed [23]. The brief primary stage in the 0.3Li and 0.4Li alloys is considered to be associated with the modest strain hardening as primary creep is dominated by strain hardening.

The creep curves of the 0.3Li and 0.4Li alloys at 37 °C under various stresses are shown in Fig. 6. Also shown in Fig. 6 are the creep curves at three different temperatures under a constant stress of 80 MPa. Both alloys exhibit substantial creep deformation at 37 °C, even under the lowest stress of 80 MPa, which corresponds to \sim 0.27 and \sim 0.22 room temperature yield strength for the 0.3Li and 0.4Li alloys, respectively. It is worth mentioning that the specimens at low stresses did not fail after \sim 40% elongation when the limit of the extensometer was reached, suggesting the possibility of superplasticity. Appreciable creep deformation is also evidenced for both alloys at room temperature (23 °C) under 80 MPa. As expected, the creep deformation is facilitated with increasing temperature from room temperature to 51 °C.

Plots of the minimum creep rate against the applied stress and reciprocal of temperature using double logarithmic coordinates for the 0.3Li and 0.4Li alloys are shown in Fig. 7a and b, respectively. Also shown are the creep data of the 0.1Li alloy [23] for comparison. It can be seen from Fig. 7a that there is a transition from power-law creep regime at low stresses to power-law breakdown regime at high stresses for all alloys. The Li content appears to have opposite influences on the minimum creep rate in the power-law creep and power-law breakdown

regimes, i.e. the minimum creep rate becomes higher with increasing Li content at low stresses but the trend is reversed at high stresses. The stress exponent in the power-law regime is found to be 2.3 for the 0.3Li and 0.4Li alloys while it is 4.1 for the 0.1Li alloy [23], suggesting that different creep mechanisms could be operating in the 0.3Li and 0.4Li alloys as in the 0.1Li alloy. This is further supported by the activation energy values determined from Fig. 7b. For the 0.1Li alloy, the creep activation energy is determined to be 87 kJ/mol, which is close to that for the lattice self-diffusion of Zn (92 kJ/mol [36]). For the 0.3Li and 0.4 alloys, however, the creep activation energy is determined to be 58 kJ/mol and 63 kJ/mol, respectively. These values are much lower than that for the lattice self-diffusion of Zn, but are close to that for the grain boundary diffusion of Zn (61 kJ/mol [36]).

The SEM fractographs of the Zn–Li alloys crept to failure at 37 °C under the same stress of 130 MPa are shown in Fig. 8. There appear different features in the fracture surface for the 0.3Li and 0.4Li alloys as compared with the 0.1Li alloy. As reported earlier [23], the fracture of the 0.1Li alloy is a mixture of intergranular and transgranular modes, evidenced by the cavities at grain boundaries and the dimple-like features. For the 0.3Li and 0.4Li alloys, no obvious grain boundary cavities can be seen in the fracture surface, but there are more dimple-like features, especially some very large dimples. Similar large dimples have been observed in the fracture surface of pure Zn with a small grain size (70 μ m) after room temperature tensile testing at a low strain rate (3 \times 10 $^{-4}$ s $^{-1}$) and were considered to result from the growth of the small dimples initiated at grain boundary triple junctions under the complex triaxial state of stress due to necking [33].

4. Discussion

4.1. Effect of Li content on the room temperature mechanical properties

On interesting result of the tensile tests is that both strength properties and ductility of the Zn–Li alloys are improved with increasing Li content, with the mechanical properties of the 0.3Li and 0.4Li alloys readily meeting the benchmark requirements for vascular stent materials. In view of the synergistic improvements in strength and ductility, the grain refinement with increasing Li content, which is revealed by the microstructural characterizations shown in Figs. 1 and 2, is considered to play an important role in influencing the mechanical properties of the current alloys. Another influencing factor is the fraction of the LiZn₄ phase, which has been related to the mechanical properties of Zn–Li alloys [6,8]. However, given that the LiZn₄ phase tends to enhance the strength properties but have a detrimental effect on ductility [6], its direct strengthening contribution is not considered to be significant for

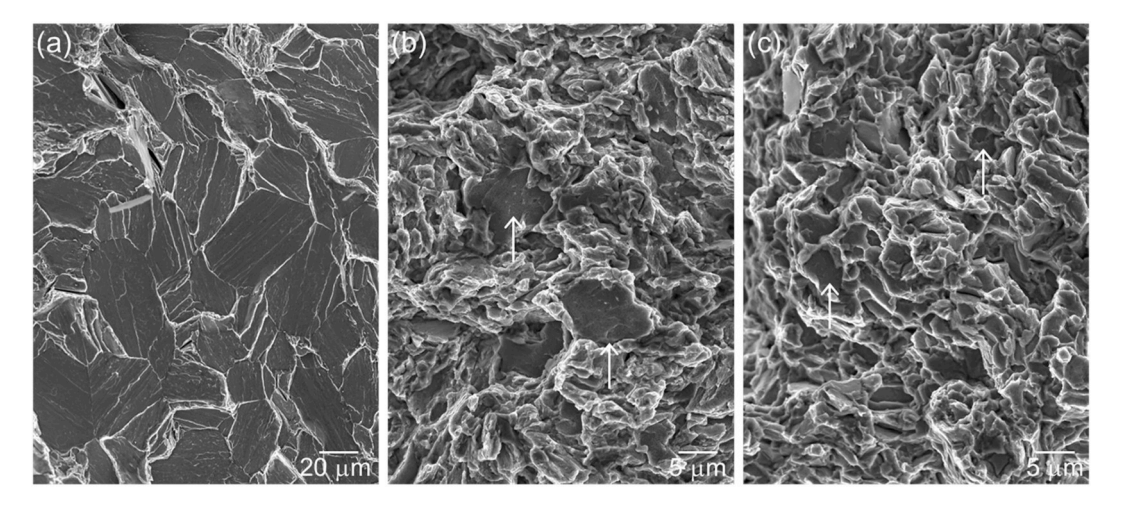


Fig. 4. SEM micrographs showing the fracture surfaces of the (a) Zn-0.1Li, (b) Zn-0.3Li and (c) Zn-0.4Li alloys after room temperature tensile testing. The arrows in (b) and (c) indicate cleavage fracture.

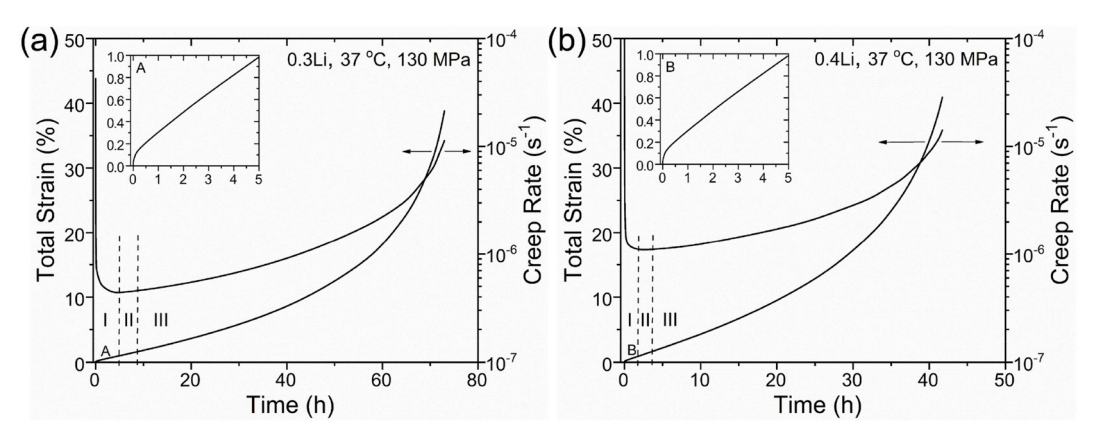


Fig. 5. Total strain and creep rate plotted against time for the (a) 0.3Li alloy and (b) at 37 °C under a stress of 130 MPa. The primary (I), secondary (II) and tertiary (III) stages are indicated. Inserted is an enlarged portion of the primary stage.

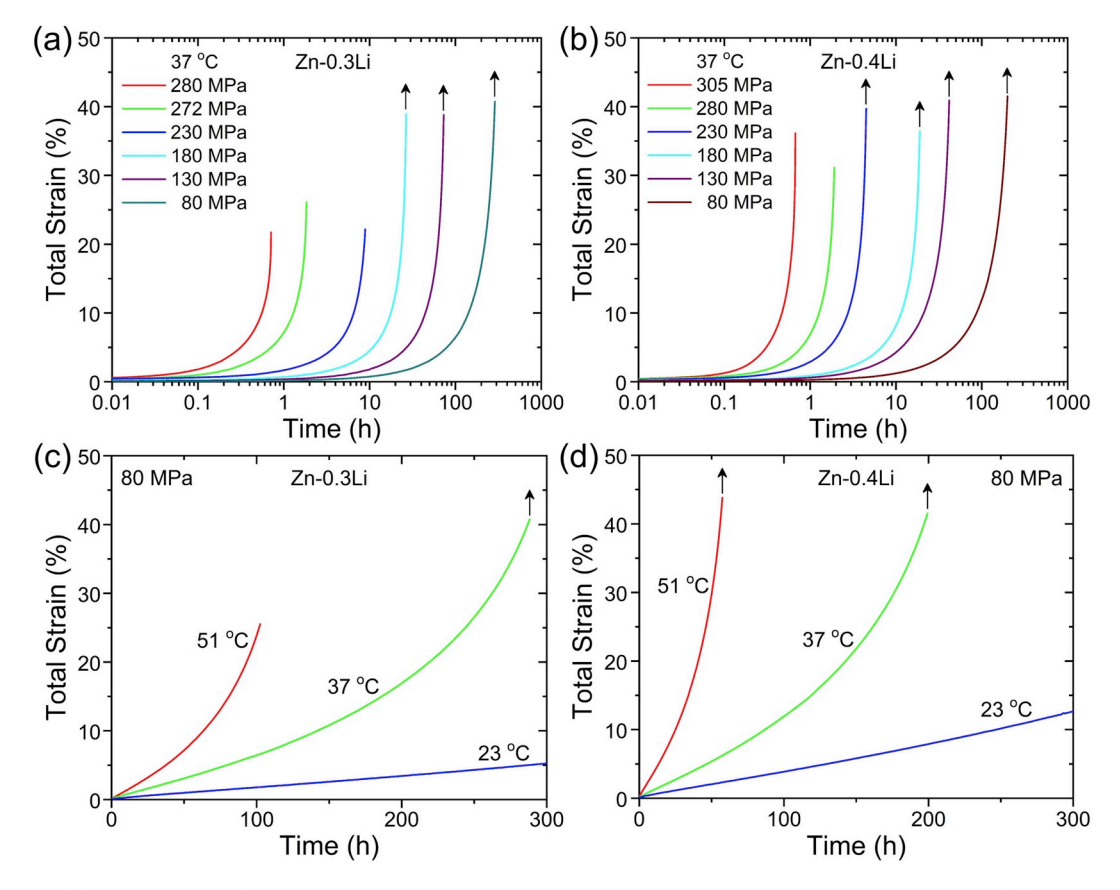


Fig. 6. Creep curves of the (a) Zn-0.3Li under various stresses at 37 °C, (b) Zn-0.4Li under various stresses at 37 °C, (c) Zn-0.3Li at different temperatures under a constant stress of 80 MPa and (d) Zn-0.4Li at different temperatures under a constant stress of 80 MPa. The arrows indicate where the limit of the extensometer was reached prior to specimen fracture.

the current Zn–Li alloys. Rather, the LiZn $_4$ phase affects the mechanical properties in an indirect way, i.e. by promoting recrystallization during the extrusion and thus grain refinement. The influence of texture is considered to be marginal in this work since there is no significant difference in texture between the current alloys.

The transition in fracture mode from the transgranular cleavage fracture in the 0.1Li alloy to the mixed transgranular cleavage and ductile dimple fracture in the 0.3Li and 0.4Li alloys also supports the important role of grain refinement in mechanical properties of the current alloys. Similar grain size effect on fracture mode has been observed in pure Zn [33] and Zn–Mg alloys [37].

Another interesting result of the tensile testsis that the strain

hardening appears to be decreased with increasing Li content. It has been realized recently [10,38] that, as vascular stent materials, Zn alloys are also required to possess a sufficient strain hardening rate to avoid strain localization since vascular stents need to undergo significant plastic deformation when radially expanded into the working state. A high strain hardening rate is expected to be beneficial for the fatigue life of vascular stents, which is at least 10 million cycles before the complete dissolution [38]. In this regard, further work is needed towards optimising the mechanical properties of Zn–Li alloys.

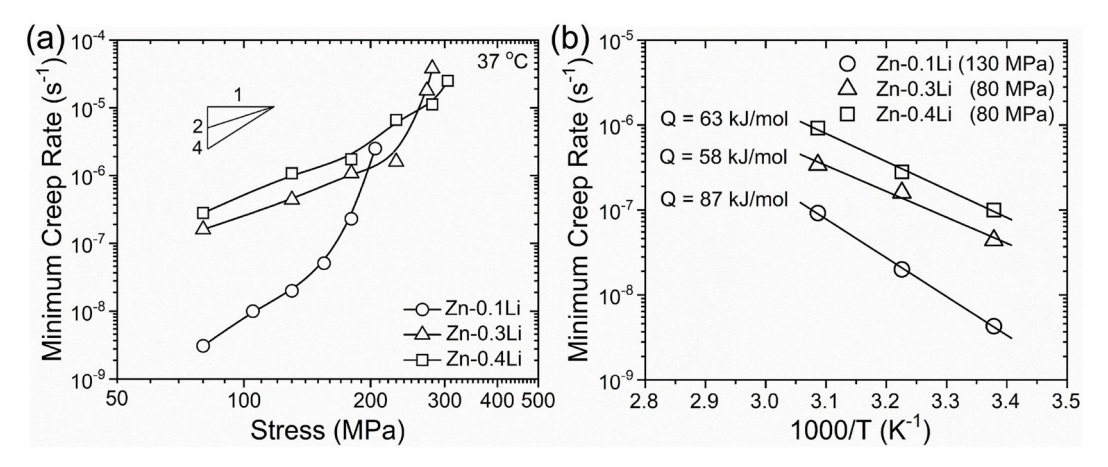


Fig. 7. Dependence of the minimum creep rate on the (a) applied stress at 37 °C and (b) testing temperature under a constant stress for the Zn-0.3Li and Zn-0.4Li alloys. The data for the Zn-0.1Li [23] are also shown for comparison.

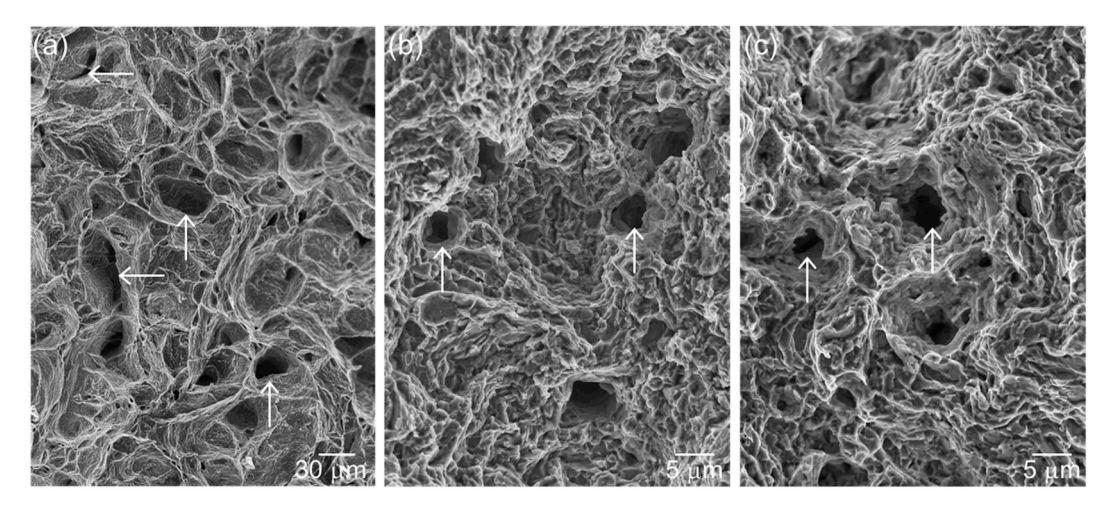


Fig. 8. SEM micrographs showing the fracture surfaces of the (a) Zn-0.1Li [23], (b) Zn-0.3Li and (c) Zn-0.4Li alloys crept to failure under a constant stress of 130 MPa at 37 °C. The horizontal arrows indicate wedge-shaped cavities at grain boundaries while the vertical arrows indicate large dimples.

4.2. Effect of Li content on the creep behaviour at human body temperature

The preceding creep results indicate that the Li content has opposite influences on the minimum creep rate in the power-law creep and power-law breakdown regimes, i.e. the minimum creep rate becomes higher with increasing Li content at low stresses but the trend is opposite at high stresses. This creep behaviour can be explained by the grain size effect. It is well known that grain boundaries are obstacles to dislocations in a crystalline material at low homologous temperatures and thus the material strength is higher at a smaller grain size, i.e. the Hall-Petch relationship. However, when temperature is sufficiently high and strain rate is sufficiently low, grain boundaries can act as effective sinks to annihilate dislocations and grain boundary hardening will turn into grain boundary softening. The transition from grain boundary hardening to softening has been extensively observed in ultrafine-grained (UFG) and nanocrystalline materials [39-41]. For the current Zn-Li alloys, the creep deformation in the power-law breakdown regime is similar to the room temperature tensile testing where the strain rate is high; in these circumstances, grain boundary hardening is believed to be predominant. In the power-law regime, however, the strain rate is much lower and grain boundary softening becomes effective.

The different stress exponent and activation energy values in the power-law regime for the current alloys suggest that different creep mechanisms could be operating in the 0.3Li and 0.4Li alloys as in the

0.1Li alloy. It has been revealed [23] that lattice diffusion controlled dislocation creep is the operative creep mechanism for the 0.1Li alloy. For the 0.3Li and 0.4Li alloys, given that the stress exponent is close to 2 and the creep activation energy is close to that for the grain boundary diffusion of Zn, grain boundary diffusion controlled grain boundary sliding is considered to be most likely the operative creep mechanism. Grain boundary sliding has been well known to be the dominant mechanism in creep and superplastic deformation of crystalline materials [42,43]. The superplastic-like deformation features of the 0.3Li and 0.4Li alloys, such as the large deformation exceeding 50% and the dimple-like features, are in support of the operation of grain boundary sliding. It has been suggested that, for ultrafine-grained materials with imperfect grain boundaries, the activation energy of grain boundary sliding should be higher than that for grain boundary diffusion, but lower than that for lattice diffusion [44]. The creep activation energy values of the 0.3Li and 0.4Li alloys seem to agree well with this mechanism.

5. Conclusions

The strength properties of pure Zn and Zn alloys in the as-cast condition cannot meet the requirements for biodegradable applications such as vascular stents. The most effective way to improving the strength properties of pure Zn and Zn alloys has been grain refinement via deformation processing, e.g. hot extrusion and hot rolling. The current

work demonstrates that, while the strength properties of Zn–Li alloys can be significantly improved by grain refinement via extrusion, such a strength improvement is not accompanied by an improvement in creep resistance at human body temperature. Actually, it is the alloy with the smallest grain size (highest strength properties) that has the poorest creep resistance. It is thus suggested that grain size of biodegradable Zn alloys needs to be controlled to achieve a balance between room temperature mechanical properties and human body temperature creep resistance.

Declaration of competing interest

The authors declare that they have no known competing financial interests or personal relationships that could have appeared to influence the work reported in this paper.

CRediT authorship contribution statement

Suming Zhu: Formal analysis, Writing - original draft. Chengcheng Wu: Formal analysis, Investigation. Guannan Li: Resources, Investigation. Yufeng Zheng: Writing - review & editing, Conceptualization, Funding acquisition. Jian-Feng Nie: Conceptualization, Methodology, Writing - review & editing.

Acknowledgements

This work was supported by Australian Research Council (ARC) through Discovery grant DP190102373 and National Natural Science Foundation of China (Grant No. 51931001). C. Wu wishes to acknowledge the Australian Postgraduate Award and International Postgraduate Research Scholarship. Monash Centre for Electron Microscopy (MCEM) is acknowledged for access to experimental facilities.

References

- H. Hermawan, D. Dube, D. Mantovani, Developments in metallic biodegradable stents, Acta Biomater. 6 (2010) 1693–1697.
- [2] Y.F. Zheng, X.N. Gu, F. Witte, Biodegradable metals, Mater. Sci. Eng. R 77 (2014) 1–34.
- [3] P.K. Bowen, J. Drelich, J. Goldman, Zinc exhibits ideal physiological corrosion behavior for bioabsorbable stents, Adv. Mater. 25 (2013) 2577–2582.
- [4] P.K. Bowen, E.R. Shearier, S. Zhao, R.J. Guillory 2nd, F. Zhao, J. Goldman, J. W. Drelich, Biodegradable metals for cardiovascular stents: from clinical concerns to recent Zn-alloys, Adv. Healthc. Mater. 5 (2016) 1121–1140.
- [5] J. Cheng, B. Liu, Y.H. Wu, Y.F. Zheng, Comparative in vitro study on pure metals (Fe, Mn, Mg, Zn and W) as biodegradable metals, J. Mater. Sci. Technol. 29 (2013) 619–627.
- [6] S. Zhao, J.-M. Seitz, R. Eifler, H.J. Maier, R.J. Guillory, E.J. Earley, A. Drelich, J. Goldman, J.W. Drelich, Zn-Li alloy after extrusion and drawing: structural, mechanical characterization, and biodegradation in abdominal aorta of rat, Mater. Sci. Eng. C 76 (2017) 301–312.
- [7] S. Zhao, C.T. McNamara, P.K. Bowen, N. Verhun, J.P. Braykovich, J. Goldman, J. W. Drelich, Structural characteristics and in vitro biodegradation of a novel Zn-Li Alloy prepared by induction melting and hot rolling, Metall. Mater. Trans. A 48 (2017) 1204–1215.
- [8] Y. Dai, Y. Zhang, H. Liu, H. Fang, D. Li, X. Xu, Y. Yan, L. Chen, Y. Lu, K. Yu, Mechanical strengthening mechanism of Zn-Li alloy and its mini tube as potential absorbable stent material, Mater. Lett. 235 (2019) 220–223.
- [9] D. Vojtech, J. Kubasek, J. Serak, P. Novak, Mechanical and corrosion properties of newly developed biodegradable Zn-based alloys for bone fixation, Acta Biomater. 7 (2011) 3515–3522.
- [10] H. Jin, S. Zhao, R. Guillory, P.K. Bowen, Z. Yin, A. Griebel, J. Schaffer, E.J. Earley, J. Goldman, J.W. Drelich, Novel high-strength, low-alloys Zn-Mg (< 0.1 wt% Mg) and their arterial biodegradation, Mater. Sci. Eng. C 84 (2017) 67–79.
- [11] E. Mostaed, M. Sikora-Jasinska, A. Mostaed, S. Loffredo, A.G. Demir, B. Previtali, D. Mantovani, R. Beanland, M. Vedani, Novel Zn-based alloys for biodegradable stent applications: design, development and in vitro degradation, J. Mech. Behav. Biomed. Mater. 60 (2016) 581–602.
- [12] H.F. Li, X.H. Xie, Y.F. Zheng, Y. Cong, F.Y. Zhou, K.J. Qiu, X. Wang, S.H. Chen, L. Huang, L. Tian, L. Qin, Development of biodegradable Zn-1X binary alloys with nutrient alloying elements Mg, Ca and Sr, Sci. Rep. 5 (2015) 10719.
- [13] A. Jarzębska, M. Bieda, J. Kawałko, Ł. Rogal, P. Koprowski, K. Sztwiertnia, W. Pachla, M. Kulczyk, A new approach to plastic deformation of biodegradable

- zinc alloy with magnesium and its effect on microstructure and mechanical properties, Mater. Lett. 211 (2018) 58–61.
- [14] S. Sun, Y. Ren, L. Wang, B. Yang, H. Li, G. Qin, Abnormal effect of Mn addition on the mechanical properties of as-extruded Zn alloys, Mater. Sci. Eng. A 701 (2017) 129–133.
- [15] Z.-Z. Shi, J. Yu, X.-F. Liu, Microalloyed Zn-Mn alloys: from extremely brittle to extraordinarily ductile at room temperature, Mater. Des. 144 (2018) 343–352.
- [16] J. Niu, Z. Tang, H. Huang, J. Pei, H. Zhang, G. Yuan, W. Ding, Research on a Zn-Cu alloy as a biodegradable material for potential vascular stents application, Mater. Sci. Eng. C 69 (2016) 407–413.
- [17] Z. Tang, J. Niu, H. Huang, H. Zhang, J. Pei, J. Ou, G. Yuan, Potential biodegradable Zn-Cu binary alloys developed for cardiovascular implant applications, J. Mech. Behav. Biomed. Mater. 72 (2017) 182–191.
- [18] M. Sikora-Jasinska, E. Mostaed, A. Mostaed, R. Beanland, D. Mantovani, M. Vedani, Fabrication, mechanical properties and in vitro degradation behavior of newly developed Zn Ag alloys for degradable implant applications, Mater. Sci. Eng. C 77 (2017) 1170–1181.
- [19] M. Wątroba, W. Bednarczyk, J. Kawałko, P. Bała, Effect of zirconium microaddition on the microstructure and mechanical properties of Zn-Zr alloys, Mater. Char. 142 (2018) 187–194.
- [20] A.H. Cottrell, V. Aytekin, Andrade's creep law and the flow of zinc crystals, Nature 160 (1947) 328.
- [21] T. Matsunaga, T. Kameyama, K. Takahashi, E. Sato, Constitutive relation for ambient-temperature creep in hexagonal close-packed metals, Mater. Trans. 50 (2009) 2858–2864.
- [22] T. Matsunaga, T. Kameyama, K. Takahashi, E. Sato, Intragranular deformation mechanisms during ambient-temperature creep in hexagonal close-packed metals, Mater. Trans. 50 (2009) 2865–2872.
- [23] S. Zhu, C. Wu, G. Li, Y. Zheng, J.-F. Nie, Creep properties of biodegradable Zn-0.1Li alloy at human body temperature: implications for its durability as stents, Mater. Res. Lett. 7 (2019) 347–353.
- [24] H. Okamoto, Desk Handbook: Phase Diagrams for Binary Alloys, ASM International, Materials Park, OH, 2010.
- [25] J. Humphreys, G.S. Rohrer, A. Rollett, Recrystallization of two-phase alloys, in: J. Humphreys, G.S. Rohrer, A. Rollett (Eds.), Recrystallization and Related Annealing Phenomena, third ed., Elsevier, Oxford, 2017, pp. 321–359.
- [26] E.R.W. Jones, W. Munro, The "elastic hysteresis" of uranium, J. Mech. Phys. Solid. 1 (1953) 182–188.
- [27] R.E. Reed-Hill, E.P. Dahlberg, W.A. Slippy, Some anelastic effects in zirconium at room temperature resulting from prestrain at 77 K, Trans. AIME 233 (1965) 1766–1771.
- [28] C.H. Cáceres, T. Sumitomo, M. Veidt, Pseudoelastic behaviour of cast magnesium AZ91 alloy under cyclic loading-unloading, Acta Mater. 51 (2003) 6211-6218.
- [29] H.Q. Ang, T.B. Abbott, S. Zhu, C. Gu, M.A. Easton, Proof stress measurement of diecast magnesium alloys, Mater. Des. 112 (2016) 402–409.
 [30] M.A. Gharghouri, G.C. Weatherly, J.D. Embury, J. Root, Study of the mechanical
- [30] M.A. Gharghouri, G.C. Weatherly, J.D. Embury, J. Root, Study of the mechanical properties of Mg-7.7at.% A1 by in-situ neutron diffraction, Phil. Mag. A 79 (1999) 1671–1695.
- [31] R.J. Werkhoven, W.H. Sillekens, J.B.J.M. van Lieshout, Processing aspects of magnesium alloy stent tube, in: W.H. Sillekens, S.R. Agnew, N.R. Neelameggham, S.N. Mathaudhu (Eds.), Magnesium Technology 2011, Springer International Publishing, Cham, 2016, pp. 419–424.
- [32] G.M. Hughes, G.E. Smith, P.E.J. Flewitt, A.G. Crocker, The brittle fracture of polycrystalline zinc, Proc. Roy. Soc. Lond. A 463 (2007) 2129–2151.
- [33] J.H. Liu, C.X. Huang, S.D. Wu, Z.F. Zhang, Tensile deformation and fracture behaviors of high purity polycrystalline zinc, Mater. Sci. Eng. A 490 (2008) 117–125.
- [34] Z. Liu, D. Qiu, F. Wang, J.A. Taylor, M. Zhang, Effect of grain refinement on tensile properties of cast zinc alloys, Metall. Mater. Trans. A 47 (2015) 830–841.
- [35] B.F. Dyson, T.B. Gibbons, Tertiary creep in nickel-base superalloys: analysis of experimental data and theoretical synthesis, Acta Metall. 35 (1987) 2355–2369.
- [36] H.J. Frost, M.F. Ashby, Deformation-Mechanism Maps: the Plasticity and Creep of Metals and Ceramics, Pergamon Press, 1982.
- [37] L.-Q. Wang, Y.-P. Ren, S.-N. Sun, H. Zhao, S. Li, G.-W. Qin, Microstructure, mechanical properties and fracture behavior of as-extruded Zn–Mg binary alloys, Acta Metall. Sin. 30 (2017) 931–940.
- [38] E. Mostaed, M. Sikora-Jasinska, J.W. Drelich, M. Vedani, Zinc-based alloys for degradable vascular stent applications, Acta Biomater. 71 (2018) 1–23.
- [39] Y.J. Li, X.H. Zeng, W. Blum, Transition from strengthening to softening by grain boundaries in ultrafine-grained Cu, Acta Mater. 52 (2004) 5009–5018.
- [40] M.A. Meyers, A. Mishra, D.J. Benson, Mechanical properties of nanocrystalline materials, Prog. Mater. Sci. 51 (2006), 427-556.
- [41] N. Ahmed, A. Hartmaier, Mechanisms of grain boundary softening and strain-rate sensitivity in deformation of ultrafine-grained metals at high temperatures, Acta Mater. 59 (2011) 4323–4334.
- [42] R. Raj, M.F. Ashby, On grain boundary sliding and diffusional creep, Metall. Trans. 2 (1971) 1113–1127.
- [43] A.K. Mukherjee, The rate controlling mechanism in superplasticity, Mater. Sci. Eng. 8 (1971) 83–89.
- [44] E.F. Dudarev, G.P. Pochivalova, Y.R. Kolobov, E.V. Naydenkin, O.A. Kashin, Diffusion-controlled true grain-boundary sliding in nanostructured metals and alloys, Mater. Sci. Eng. A 503 (2009) 58–61.